

A Quantum Electrodynamics Kondo Circuit with Orbital and Spin Entanglement

Guang-Wei Deng^{†,1,2} Loïc Henriët^{†,3} Da Wei,^{1,2} Shu-Xiao Li,^{1,2} Hai-Ou Li,^{1,2} Gang Cao,^{1,2}
Ming Xiao,^{1,2} Guang-Can Guo,^{1,2} Marco Schiró,⁴ Karyn Le Hur,³ and Guo-Ping Guo^{1,2,*}

¹Key Laboratory of Quantum Information, University of Science and Technology of China,
Chinese Academy of Sciences, Hefei 230026, China

²Synergetic Innovation Center of Quantum Information & Quantum Physics,
University of Science and Technology of China, Hefei, Anhui 230026, China[†]

³Centre de Physique Théorique, École polytechnique,
CNRS, Université Paris-Saclay, F-91128 Palaiseau, France[†]

⁴Institut de Physique Théorique, Université Paris Saclay, CNRS, CEA, F-91191 Gif-sur-Yvette, France

(Dated: October 16, 2015)

Recent progress in nanotechnology allows to engineer hybrid mesoscopic devices comprising on chip an artificial atom or quantum dot, capacitively coupled to a microwave (superconducting) resonator. These systems can then contribute to explore non-equilibrium quantum impurity physics with light and matter, by increasing the input power on the cavity and the bias voltage across the mesoscopic system. Here, we build such a prototype system where the artificial atom is a graphene double quantum dot (DQD). Controlling the coupling of the photon field and the charge states of the DQD, we measure the microwave reflection spectrum of the resonator. When the DQD is at the charge degeneracy points, experimental results are consistent with a Kondo impurity model entangling charge, spin and orbital degrees of freedom. The light reveals the formation of the Kondo or Abrikosov-Suhl resonance at low temperatures. We then study the complete phase diagram as a function of gate voltages, bias voltage and microwave input power.

I. INTRODUCTION

Circuit quantum electrodynamics (cQED) with quantum dot geometries has gained rapid development recently [1–24] offering a platform to address interaction effects between photons and electrons on-chip. These settings typically involve an electronic nano-circuit, such as a single or double quantum dot (DQD) coupled to source/drain leads and to an electromagnetic resonator. A bias applied across the nanocircuit can cause a current flowing as well as dissipation, which will result in challenging physics when coupled to a photon field. These hybrid systems are not only of great practical relevance for quantum information technology [2, 12, 25] but also of fundamental interest as platforms to explore exotic quantum impurity physics with light and matter [26]. In this respect DQD-resonator devices are particularly interesting, as they allow deep quantum limit transport investigations, including electronic entanglement [8, 11, 18–20], DQD maser [10, 22, 23], photon emission statistics [22, 23] and heat engines [14]. From a more fundamental perspective, a DQD may host interesting degenerate states, entangling charge, spin and orbital degrees of freedom, which can turn through quantum fluctuations into exotic many body states [27–39]. We note recent progress concerning the strong coupling of spin to photons through artificial spin-orbit interactions [40] or polarization rotation [41]. Out of equilibrium charge dynamics in a hybrid cQED architecture [15], and photon emission from a cavity-coupled DQD [10, 42] have been

reported. In this paper we present evidence for exotic Kondo correlations in the microwave response of a DQD-cavity coupled to leads, a unique signature of many-body quantum impurity physics with light, which has not yet been achieved in these hybrid devices.

We probe the response of a DQD-resonator device by measuring phase and amplitude of the reflected microwave signal as a function of bias and gate voltages as well as the response of the resonator as a function of the input microwave power. Our data reveal how unique features of the electronic transport appear in the photon spectroscopy. In particular at the charge degeneracy points of the DQD, the phase response of the reflected light signal in this geometry shows a robust π phase shift upon increasing the bias voltage up to a threshold set by the charging energy, while the amplitude response shows additional satellite peaks at low bias. We show that the experimental findings are in qualitative agreement with an effective light-matter quantum impurity model in relation with Kondo physics [43]. More precisely, we extend the Kondo model in Ref. [27] applied to the DQD at the charge degeneracy points to the case of graphene DQD. SU(4) Kondo effect was recently observed in a GaAs double quantum dot [44]. We justify that the decoupling of the antisymmetric wave-function in terms of the two graphene sub-lattices leads to a fully screened SU(4) Kondo model in the low-temperature limit. We will show how the experimental data are consistent with this interpretation at very low temperatures. We shall also discuss temperature effects. We will also assume that the chemical potential does not lie at the charge neutrality point in the graphene leads, and justify this assumption. For an introduction on Kondo physics, see Refs. [45–51]; for Kondo physics in quantum dots, consult Refs. [52–56].

* Corresponding author: gpguo@ustc.edu.cn

[†] These authors contributed equally to this work.

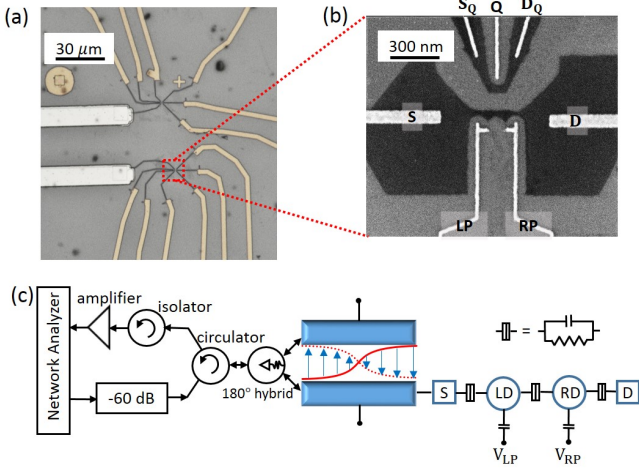


FIG. 1. (color online). (a) Micrograph of the DQD gate structure. (b) Sample structure of a typical etched graphene DQD. The dc voltages used to control the charge numbers in the DQD are applied via left and right plunger (LP and RP) gates. A quantum point contact with a source (S_Q) and drain (D_Q) channel and a tuning gate (Q) is integrated near the DQD. (c) Circuit schematic of the hybrid device. The half-wavelength reflection line resonator is connected to DQD's left dot (LD) at one end of its two stripelines. The right dot (RD) is connected to the drain. A microwave signal is applied to the other end of the resonator, and the reflected signal is detected using a network analyzer.

To our knowledge, our paper constitutes the first report of the realization of Kondo physics with graphene double dots at the charge degeneracy point exhibiting charge and spin entanglement [27]. Previous works on graphene double quantum dots were carried both in series shape [57] and in parallel [58]. The Kondo effect has also been observed in graphene with point defects (vacancies) [59]. Similar to a three-lead or four-lead geometry [44, 60], the cavity which is weakly-coupled to the mesoscopic system, allows to reveal certain aspects of the spectral function on the DQD. Josephson-Kondo circuits have also been proposed to probe Kondo physics of light [61–63]. We note related progress from the experimental point of view both in cQED [64–66] and in mesoscopic systems [67].

Our device (shown in Fig. 1) is mounted in a dry dilution refrigerator, its base temperature is about 30 mK. Two DQDs, made of few-layer etched graphene, are coupled to the resonator through their sources [11], however, only one of them is used in this experiment while the other is grounded all over the experiment. A vector network analyzer (VNA) is used to apply coherent microwave driving tone and measure the reflection signal (see Fig. 1(c)).

The DQD may have several effects on the resonator: dispersive effects [5, 9] can cause a shift on the resonance frequency as well as dissipation effects [6]. Derived from the input-output theory [71, 72], the reflection coefficient

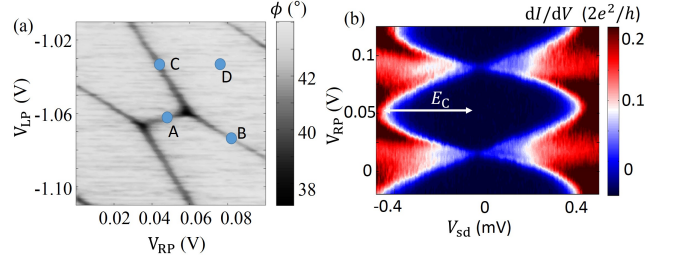


FIG. 2. (color online) (a) Charge stability diagram of the DQD measured by the dispersive readout using the resonator and (b) Coulomb diamond measured by transport experiment and revealing the charging energy. The gate lever arms are $\sim 10\%$.

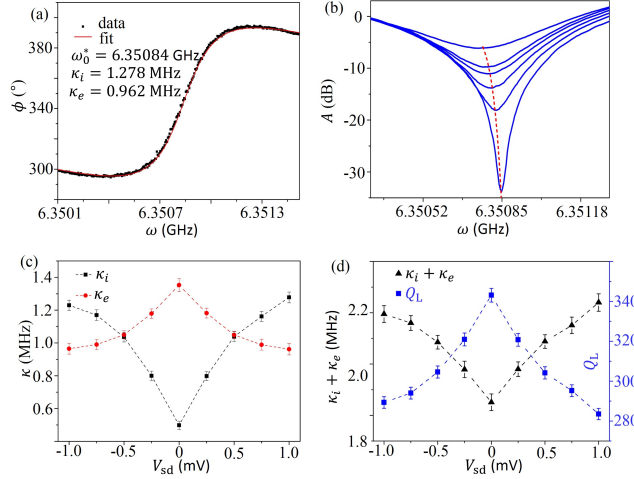


FIG. 3. (color online) Results for point A. (a) Best fit of the phase as a function of the frequency when DQD bias voltage $V_{sd}=1$ mV, from which the resonance frequency ω_0^* , κ_i and κ_e can be obtained. (b) Amplitude response as a function of the driving frequency, for various bias voltages (0, 0.5, 0.6, 0.7, 0.8, 1 mV). The red dashed line shows the fitted resonance frequency, shifted by the electron transport. (c) κ_i and κ_e as functions of the DQD bias voltage. (d) Total dissipation and load quality factor $Q_L = \omega_0^*/(\kappa_i + \kappa_e)$ as a function of the bias voltage.

of the resonator is defined as [9, 73]:

$$S_{11}(\omega) = \frac{i(\omega_0^* - \omega) + \frac{\kappa_i - \kappa_e}{2}}{i(\omega_0^* - \omega) + \frac{\kappa_i + \kappa_e}{2}}, \quad (1)$$

where ω is the driving frequency, ω_0^* is the cavity resonance frequency (taking into account the shift from the coupling with the mesoscopic system), κ_e represents the dissipation mechanisms from the light-matter coupling and κ_i incorporates the dissipation from the photon system only. In the present experiment, these parameters can be explicitly tuned with the bias voltage applied across the mesoscopic system and a precise analysis will be required to fit the experimental datas. The total dissipation rate on the cavity is $\kappa = \kappa_i + \kappa_e$.

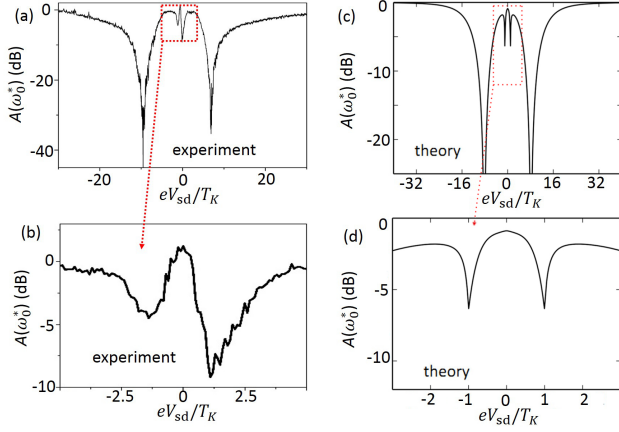


FIG. 4. (color online) Results for point A, for the amplitude of the reflection coefficient $S_{11}(\omega_0^*)$ as a function of the source-drain bias; the zoom focuses on low-energy Kondo features. Theory results based on an effective quantum impurity model. We take $T_K = 550\text{mK}$ (extracted from the temperature analysis) and $E_c = 0.4\text{meV}$ from Fig. 2, $\omega_0 = 6\text{GHz}$, $\lambda/\omega_0 = 2.10^{-2}$, $\alpha = 3.10^{-3}$ and $\epsilon_0 = T_K$. For $|V_{sd}| > T_K$, we model decoherence effects on the Kondo resonance with a (decoherence) rate $\Gamma(V_{sd})$ which grows rapidly with $|V_{sd}|$ [68–70] and saturates around E_c .

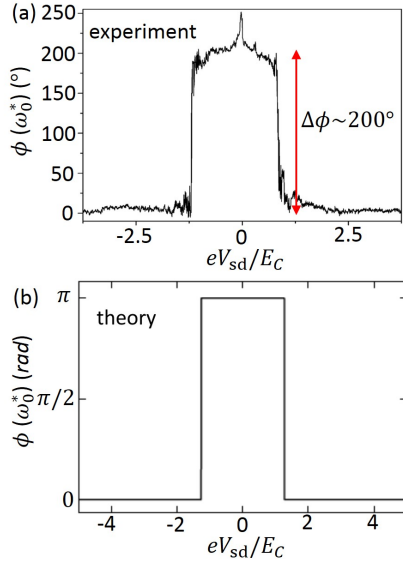


FIG. 5. (color online) Experimental and Theory results for the phase of $S_{11}(\omega_0^*)$ at Point A. The phase behavior (roughly π or 0) can be understood from the evolution of κ_e and κ_i with the bias voltage.

S_{11} can be measured by its amplitude ($A = |S_{11}|$) and phase ($\phi = \arg(S_{11})$) components or by the imaginary ($\Im m(S_{11})$) and real ($\Re e(S_{11})$) parts through the VNA. We then set the DQD to different states, to see the effect of the DQD on the resonator. We can first obtain a charge stability diagram of the DQD by a dispersive readout measurement [5, 9][see Fig. 2(a)]. The Coulomb

diamond in Fig. 2(b) is obtained from transport measurements.

In Figure 3, we plot the amplitude and phase response as a function of the driving frequency at point A. Using a fit with Eq. (1), we can deduce ω_0^* , κ_i , and κ_e [9, 73] and their evolution with respect to the bias voltage. Fitting the $V_{sd}=0$ curve, we obtain $\omega_0^*(V_{sd} = 0) = 6.35080\text{GHz}$, $\kappa_i(V_{sd} = 0) = 0.498\text{MHz}$ and $\kappa_e(V_{sd} = 0) = 1.353\text{MHz}$. For $V_{sd} = 1\text{mV}$ curve, we obtain $\omega_0^*(V_{sd} = 1\text{mV}) = 6.35084\text{GHz}$, $\kappa_i(V_{sd} = 1\text{mV}) = 1.278\text{MHz}$ and $\kappa_e(V_{sd} = 1\text{mV}) = 0.962\text{MHz}$ (Fig. 3(a)). Compared to the $V_{sd}=0$ curve, there is a 40 KHz frequency shift, which is caused by the nonlinearities induced by the nonlinear electronic transport [26]. Figure 3(c) shows the comparison of κ_i and κ_e for various bias voltages. From zero bias to $V_{sd}=1\text{mV}$, κ_i increases by 0.78 MHz and κ_e decreases by 0.391 MHz. In this description, κ_i and κ_e do not depend on the frequency.

II. THE CHARGE DEGENERACY POINT

A. Experimental Results

Now we discuss additional experimental results for point A, at the resonance frequency ($\omega = \omega_0^*$). Figures 4 and 5 show the evolution of the amplitude and phase response at the resonance frequency with respect to the bias voltage.

A phase shift $\Delta\phi \simeq \pi$ is observed from bias voltage $V_{sd} \sim 0$ to $V_{sd} \sim \pm 0.4\text{mV}$. The behavior of the phase response can be understood from very general arguments and Eq. (1). Indeed at small bias voltages, one expects that the coupling of the cavity resonator with the electronic system is large then producing $\kappa_e \gg \kappa_i$ and a phase of π in the reflected microwave signal. On the other hand, at large bias voltages, the current through the DQD should be large such that the dynamics of the electronic degrees of freedom is much faster than the dynamics of the photon resulting in $\kappa_e \ll \kappa_i$ and a phase which is zero (or 2π) [26]. This relatively simple argument allows to explain the phase shift of $-\pi$ (π) in the reflected microwave signal when increasing the bias voltage across the mesoscopic electron system, and the datas of Figure 3(c) confirm this evolution. The amplitude (in dB) shows also two pronounced dips around $V_{sd} \sim \pm 0.4\text{mV}$, which is consistent with this argument.

It is important to note two points concerning these measurements. First, the absolute value of the voltage corresponding to the phase shift and the amplitude dips corresponds to the charging energy $E_c \sim 0.4\text{meV}$ of the DQD measured through dc transport and leading to the Coulomb diamond (see Fig. 2(b)). Interestingly, we also notice the low bias regime shows a (slightly asymmetric) dip structure (see Fig. 4(b)). As explained below, we attribute the low bias dip structure as well as

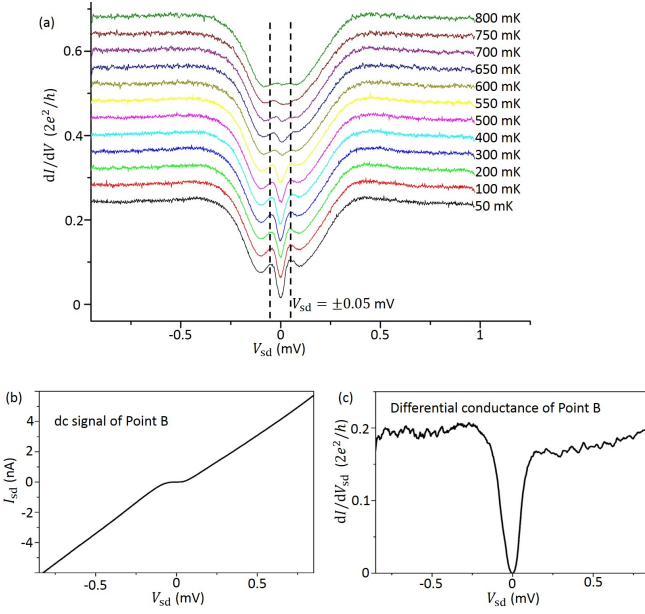


FIG. 6. (color online) Upper panel: temperature evolution of the differential conductance at point A, showing two peaks at finite voltage $V_{sd} \sim \pm 0.05 \text{ mV}$ and a zero bias dip corresponding to a small residual conductance, which smoothly disappears above a crossover Kondo temperature of about $T_K \sim 550 \text{ mK}$. Curves are displaced from the base reference by a constant offset. For an $SU(4)$ Kondo model, the zero-bias anomaly in the conductance does not occur at $V_{sd} \rightarrow 0$, but rather at voltages in relation with Kondo physics [29]. The Kondo anomalies disappear at a temperature scale $T_K \sim 550 \text{ mK}$. In addition, when $V_{sd} \rightarrow 0$, at low temperatures, one predicts $G_0 = dI/dV(V_{sd} = 0) \sim (t'/T_K)^2 2e^2/h$ [27] which confirms that $t' \sim 0.1 - 0.3 T_K \ll T_K$. Lower panels: Current (a) and differential conductance (b) at point B at $T=30 \text{ mK}$, showing no zero-bias anomaly.

the robustness of the π phase (at low temperatures) to Kondo physics. A phase of $\pi = 2 \times \pi/2$ is expected in the reflected light wave, associated with a bound state formation [43]. This phase of π is not in disagreement with the phase of $\pi/2$ in the transmission predicted in Ref. [26].

For completeness, we also present in Fig. 6 the transport datas at the points A and B (and the evolution of the transport datas with respect to temperature for the case of point A). At the charge degeneracy point A, these measurements show at low temperatures a very rich small-bias structure, well inside the charging energy bands, with two peaks at finite voltage $V_{sd} \sim \pm 0.05 \text{ mV}$ and a zero bias dip corresponding to a finite small residual conductance. Upon heating these features smoothly disappear above a crossover temperature of about 550 mK . In Fig. 7 and 8, we show the temperature evolution of the amplitude and phase of the reflected signal. In this cooling procedure, the effective electrical sample temperature is around 100 mK whereas the sample environment temperature of the dilution

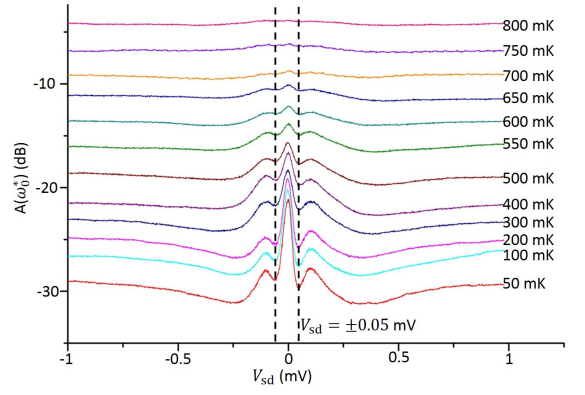


FIG. 7. (color online) Temperature dependence of the microwave reflected signal amplitude at point A. Curves are displaced from the base reference by a constant offset. (We emphasize that in this cooling procedure, the effective electrical temperature of the sample is around 100 mK whereas the dilution refrigerator temperature T can reach lower temperatures. The datas do not change much on the figure for temperature T smaller than 100 mK .)

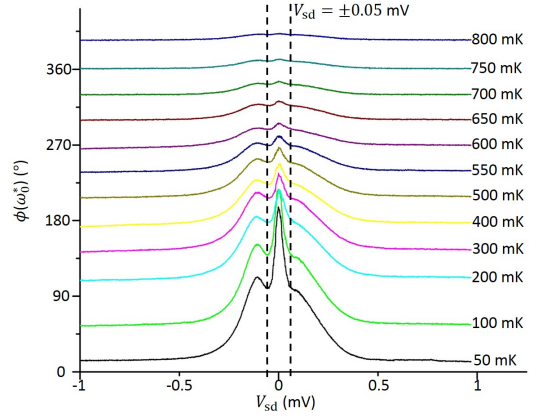


FIG. 8. (color online) Evolution of the phase of the microwave reflected signal at point A. The cooling procedure is similar to that used in Fig. 7 for the amplitude. Interestingly, one observes that the phase converges to π for $T < T_K = 550 \text{ mK}$ for $V_{sd} \rightarrow 0$ and that the phase evolution is sensitive to the Kondo temperature. In addition, experimentally, for intermediate temperatures (we remind that the effective electrical temperature of the sample is around 100 mK in this cooling procedure), the phase smoothly drops to zero for $|V_{sd}| > T_K$.

refrigerator can reach lower temperatures. Therefore, the datas of Fig. 6, Fig. 7 and Fig. 8 do not evolve much for temperatures of the refrigerator below 100 mK .

B. Exotic Spin and Orbital Kondo model

To support the experimental results, we provide a theoretical model to describe the precise evolutions of κ_e

and κ_i with the bias voltage.

At the point A, the two low lying charging states (1, 0) and (0, 1) — with one electron either on the left or on the right dot — are degenerate since it costs the same energy to have one extra electron on the left or on the right dot [74]. Other configurations on the DQD cost higher energy. The low-energy theory can then be built by introducing, in addition to the spin $S^z = \pm 1/2$ of the electron delocalized on the DQD, the orbital pseudospin quantum number $T^z = \pm 1$, projecting on these two allowed states which are further coupled by a finite tunneling term $t'T^x$. These four quantum states of the DQD generate exotic Kondo physics when coupled to the two channels conduction electrons.

As a result of second-order tunneling processes, the electron leads are coupled through the Hamiltonian $H_1 = H_{kin} + H_{kondo} + H_{assist} + H_{orbital}$ [27]. Here, H_{kin} represents the kinetic energy in the two leads. Second-order tunneling processes are classified through purely Kondo terms involving spin flips, orbital contributions changing the lead index from say $l = L$ (left) to $l = R$ (right) and flipping the charge state on the DQD, and assisted tunneling processes entangling the charge and spin [27]:

$$H_{Kondo} + H_{assist} = \frac{J}{2} \bar{S} \psi^\dagger \bar{\sigma} \psi + Q_z T^z \bar{S} \psi^\dagger \tau^z \bar{\sigma} \psi \quad (2)$$

$$+ Q_\perp \left(T^+ \bar{S} \psi^\dagger \tau^- \bar{\sigma} \psi + h.c. \right)$$

$$H_{orbital} = \frac{1}{2} (V_z T^z \psi^\dagger \tau^z \bar{\sigma} \psi + V_\perp (T^+ \psi^\dagger \tau^- \bar{\sigma} \psi + h.c.)),$$

where $\psi_{\sigma l}$ is the Fourier transform of $c_{k\sigma l}$ which refers to an electron operator with spin σ in lead l . Here, \bar{S} corresponds to the spin operator of the electron delocalized on the DQD, $\bar{\sigma}$ and $\bar{\tau}$ act on the spin space and orbital (lead) space of the electron operators. The couplings above can be written in terms of the tunneling rate to the right/left lead Γ_\pm and the charging energy of the DQD E_c respectively as [27] $J = Q_z = (\Gamma_+ + \Gamma_-)/4E_c$, $Q_\perp = V_\perp = \sqrt{\Gamma_+ \Gamma_-}/E_c$.

The model presented here from Ref. [27] can be explicitly refined to incorporate the precise geometry of the graphene lattice (leads)[75]. Let us consider the two sub-lattices of the honeycomb lattice A and B . The above analysis remains valid assuming that the symmetric wave-function $\psi_{\sigma l} = 1/\sqrt{2}(\psi_{A\sigma l} + \psi_{B\sigma l})$ couples to the double dot through second order tunneling processes, whereas the anti-symmetric component would be disconnected from the double dot and therefore can be ignored.

The kinetic term leading to a Dirac type linear dispersion can also be diagonalized in this basis if we assume a symmetric configuration for the A and B sites with respect to the direction of the tunneling. The use of either open or periodic boundary conditions in the orthogonal direction then lead to a one-dimensional kinetic Hamiltonian along the direction of the tunneling, which is diagonal in this basis [76, 77]. We argue that a small geometrical asymmetry is unimportant, as the symmetric term would dominate in the renormalization procedure.

Below, we assume that the density of states in graphene is finite, meaning that the chemical potential does not lie at the charge neutrality point where the density of states vanishes (The Kondo temperature would vanish, which does not seem in agreement with experimental results).

As shown in Ref. [27] and in related models [28–30], this DQD model at point A flows to a Kondo-type fixed point with a Fermi liquid ground state [78–80], which is quite robust to (charge) noise effects [81]. Experiments have reported the possible occurrence of an emergent $SU(4)$ symmetry at the low-energy fixed point, in similar geometries, due to the entanglement between spin and orbital degrees of freedom [31–35]. The remarkable fact is that the bare parameters Γ_+ and Γ_- are replaced by a single parameter describing the low-energy fixed point, namely the Kondo energy scale T_K . In this description the spectral function of the DQD can be modeled by an effective resonant level model [29], associated with spinless fermionic operators d and d^\dagger . These operators d and d^\dagger are defined in correspondance with the processes involving the orbital operators T^- and T^+ respectively. This spinless description is legitimate as the two spin components add up in the conductance, and the cavity is only sensitive to the orbital degree of freedom. In this strong coupling regime, the system can then be treated by analogy with the case of one single dot studied in Ref. 26, the only difference being that the position ϵ_0 and the width Γ of the electronic level are determined by the $SU(4)$ fixed point. At small bias voltages $V_{sd} \leq T_K$, the Kondo resonance is described by the spectral function [29]:

$$\rho(\omega) = \frac{1}{\pi} \frac{T_K}{(\omega - \epsilon_0)^2 + T_K^2}, \quad (3)$$

where ϵ_0 is of the order of T_K [29, 80]. We stress that even though we describe the effective resonant level with spinless operators, the spin of the electrons is a highly relevant quantity: the joint effect of the orbital and spin degrees of freedom lead to a Kondo resonance at ϵ_0 of the order of T_K , above the Fermi surface. In contrast, a purely spin Kondo effect would yield $\epsilon_0 = 0$, and transport properties would be very distinct.

We first remark that the DC transport datas exposed in Fig. 6 is in accordance with our model. The transport datas for the point A indeed yield a zero-bias anomaly at $V_{sd} \sim \pm T_K$ (see the upper pannel of Fig. 6), which is consistent with this form of the spectral functions, with ϵ_0 above the Fermi energy of the reservoir electron leads. The conductance across the DQD at small bias voltages essentially follows $2e^2/h T_K \rho(\omega = e|V_{sd}|)(t'/T_K)^2$, where h is the Planck constant and T_K is the Kondo energy scale. The spectral function gives the density of states accessible for an incoming electron, the prefactor $(t'/T_K)^2$ corresponds to the transition probability between the two dots. This also leads to a finite conductance at $V_{sd} \rightarrow 0$, as observed in Fig. 6. In the Kondo limit, one predicts a differential conductance $G_0 = dI/dV(V_{sd} = 0) \sim (t'/T_K)^2 2e^2/h$ [27], which leads

to the prediction $t' \sim 0.1 - 0.3T_K$. In addition, the $SU(4)$ Kondo theory predicts that the conductance evolves (increases) linearly with the bias voltage for $V_{sd} \rightarrow 0$ [29], as found in the experiment (Fig. 6). From the temperature analysis of the datas, we also infer that the Kondo energy scale T_K , at which the zero-bias peaks in the differential conductance (Fig. 6) and the low-bias features disappear in the light reflected signal (Fig. 7 and Fig. 8) is roughly around $550mK$.

By contrast, the differential conductance at point B does not show such anomaly at $V_{sd} \sim \pm T_K$, as can be seen in the two lower pannels of Fig. 6. At point B, the levels of the two dots are not degenerate : this energy splitting is the analog of an orbital magnetic field along the z direction, which suppresses the orbital Kondo effect and suppresses the conductance at $V_{sd} \rightarrow 0$.

C. Light-Matter Coupling

The cavity and light-matter coupling are described through the Hamiltonian

$$H_2 = \omega_0 a^\dagger a + \lambda \left[\sum_{k\sigma} c_{k\sigma L}^\dagger c_{k\sigma L} \right] (a + a^\dagger), \quad (4)$$

where we fix the Planck constant $\hbar = h/(2\pi)$ to unity. The cavity is capacitively coupled to the left lead only. The key point is that one can re-write the light-matter coupling as a quantum dot-cavity coupling of the form $\lambda T^z (a^\dagger + a)$. To show this, one can apply a unitary transformation $U = \exp \left[i\phi \left(\sum_{k\sigma} c_{k\sigma L}^\dagger c_{k\sigma L} + T^+ T^- \right) \right]$ with $\phi = \frac{\lambda(a - a^\dagger)}{i\omega_0}$ on the Hamiltonian $H = H_1 + H_2 + t'T^x$.

The part of the transformed Hamiltonian involving the cavity takes the form:

$$\tilde{H}_{cav} = t'(T^- e^{i\phi} + T^+ e^{-i\phi}) - \lambda T^z (a + a^\dagger) + \omega_0 a^\dagger a \quad (5)$$

The phase factor entering the tunnel coupling between the dots appears in fact at all the investigated points in the phase diagram; the total Hamiltonian then reads $\tilde{H} = H_1 + \tilde{H}_{cav}$, see Appendix A.

We can proceed and compute the reflection coefficient using the input-output theory [71, 72]. The input power couples to the $\hat{x} \propto (a + a^\dagger)$ variable of the cavity. Therefore, at small input power, the reflection coefficient reads [61]:

$$S_{11}(\omega, V_{sd}) = -1 + 2iJ(\omega)\chi_{xx}^R(\omega, V_{sd}). \quad (6)$$

The susceptibility for the photon as well as the photon self-energy are defined as [26]

$$\chi_{xx}^R(\omega) = \frac{\omega_0}{\omega^2 - \omega_0^2 - \omega_0 \Pi^R(\omega) + iJ(\omega)\omega_0}, \quad (7)$$

where the photon self-energy $\Pi^R = \Re \Pi^R - i\Im \Pi^R$ absorbs the light-matter coupling. Using these identifications, for frequencies close to ω_0^* , we recover Eq. (1) with

$\kappa_i = J(\omega_0^*(V_{sd})) = 2\pi\alpha\omega_0^*$ and $\kappa_e = \Im m \Pi^R(\omega_0^*)$. At zero temperature, the function $J(\omega)$ describes explicitly the dissipation of the cavity mode due to the coupling with the long transmission line which transports the input signal (and we can safely neglect the effect of the small number of photons produced in the cavity for voltages larger than T_K due to the current flowing across the dot [26]). Theoretically, we assumed the specific form $J(\omega_0^*(V_{sd})) = 2\pi\alpha\omega_0^*$ which is typical of a transmission line (ohmic bath) in the quantum limit [82–88] (with an ultraviolet frequency cutoff much larger than T_K); α is a dimensionless parameter proportional to the resistance of the transmission line. The coupling between the left quantum dot and the cavity produces an extra dissipation source for the cavity. In the text above, the cavity frequency is defined auto-coherently by

$$\omega_0^*(V_{sd})^2 = \omega_0^2 + \omega_0 \Re \Pi^R[\omega_0^*(V_{sd})]. \quad (8)$$

The measurements of the renormalized resonance frequency carried out on our device match well the theoretical expectations. We note in particular that $\omega_0^*(V_{sd}) < \omega_0$ increases with V_{sd} — reflecting that $\Re \Pi^R$ becomes less important — and tends to ω_0 at large bias [26], as can be seen in Fig. 3(b). This also implies that $J(\omega_0^*)$ or κ_i becomes more substantial when increasing the bias voltage, as experimentally confirmed in Fig. 3(c). In addition, from the experimental Fig. 3(b) and formula (7), we estimate roughly the light-matter coupling $\lambda/\omega_0 \sim 2.10^{-2}$ which justifies the perturbative analysis above.

D. Effective Quantum Impurity Model description of Photon Transport

Computing the photon self-energy for the exotic spin-orbital photonic Kondo model introduced in the previous section is a challenging task. To proceed we use the fact that the electronic sector flows to a Kondo-Fermi liquid fixed point [28–30], where the spectral function on the DQD can be modeled by an effective resonant level model, as exposed previously. We take a bias dependent width Γ to include voltage induced decoherence effects [68, 69] on the pseudo-fermion d . We then show thanks to Keldysh perturbation theory [26] that the photon self-energy $\Pi^R = \Re \Pi^R - i\Im m \Pi^R$ is related to the density-density response function of a purely electronic Anderson Impurity Model. We have at second order in the light-matter coupling

$$\Pi^R(\Omega) = \frac{-i\lambda^2}{2} \int \frac{d\omega}{2\pi} [G_0^R(\omega)G_0^<(\omega - \Omega) + G_0^A(\omega)G_0^<(\omega + \Omega)], \quad (9)$$

where G_0^R , G_0^A and $G_0^<$ are respectively the Retarded, Advanced and Lesser Green's functions of the electronic level associated to the Kondo resonance. Using this description of the spectral function [89] on the DQD we evaluate the photon self energy $\Im m \Pi^R(\omega_0^*, V_{sd})$ at the

renormalized resonance frequency $\omega_0^*(V_{sd})$ [26]

$$\begin{aligned} \Im m \Pi^R(\omega_0^*) &= \lambda^2 f_\Gamma(\omega_0^*) \sum_{\alpha, a=\pm} \alpha \arctan \left(\frac{\mu_a - \epsilon_0 + \alpha \omega_0^*}{\Gamma} \right) \\ &+ \lambda^2 f_\Gamma(\omega_0^*) \sum_{\alpha, a=\pm} \frac{\Gamma}{\omega_0^*} \ln \left(\frac{(\mu_a - \epsilon_0 + \alpha \omega_0^*)^2 + \Gamma^2}{(\mu_a - \epsilon_0)^2 + \Gamma^2} \right), \end{aligned} \quad (10)$$

where $f_\Gamma(\omega_0^*) = \Gamma / (4\pi^2 \Gamma^2 + \pi^2 \omega_0^{*2})$, $\mu_a = aV_{sd}/2$ and Γ is bias-dependent: $\Gamma = T_K$ the Kondo energy scale (of the order of ω_0^*) at small biases and is an increasing function of V_{sd} to account for bias-induced decoherence effects [68–70], with $\Gamma \sim V_{sd} / \log^2(V_{sd}/T_K)$ for $V_{sd} \gg T_K$.

The expression of the imaginary part of the self-energy respects the (particle-hole) symmetry $V_{sd} \rightarrow -V_{sd}$, as the total dissipation in the system is the sum of the dissipation coming from electronic and hole processes. We also remark that $\Im m \Pi^R$ becomes substantial for $\Gamma \simeq \omega_0^*$. In this regime, and for $\epsilon_0 \simeq \Gamma$, this even function goes to zero rapidly for $|V_{sd}| \geq 2\Gamma$. This behaviour is responsible for the dips that occur for $V_{sd} \sim \pm \Gamma \sim \pm T_K$ in Fig. 4, as the dissipation stemming from the electronic system decreases. For $|V_{sd}| \geq T_K$, Γ is an increasing function of V_{sd} , allowing $\Im m \Pi^R(\omega_0^*)$ to remain substantial, leading to a robust π phase in the reflected signal. For bias voltages close to $E_c \sim 0.4 \text{ meV}$ the model ceases to be valid because other energy levels such that $(1, 1)$ or $(0, 0)$ can be involved. Therefore, in the theory, we include the fact that Γ saturates to a large value close to the ultra-violet cutoff E_c . The Kondo resonance has almost collapsed due to a very short life-time for $V_{sd} \sim E_c$.

For an $SU(4)$ Kondo effect, one predicts $\epsilon_0 \sim T_K$ and for an $SU(2)$ Kondo effect (which is equivalent to a broken $SU(4)$ symmetry onto a lower $SU(2)$ spin symmetry), one gets $\epsilon_0 = 0$ [29, 80]. Here, the theory fits the experimental results for $\epsilon_0 = T_K$ (Fig. 4).

As shown in Figs. 4 and 5, this analysis successfully corroborates the experimental results at point A. For small bias voltages, the photon field is sensitive to the Kondo physics producing $\kappa_e \gg \kappa_i$ and a phase shift close to π in the microwave reflected signal. Interestingly, the decoherence effects induced by the bias voltage enlarge the value of Γ for $V_{sd} \geq T_K$, which corresponds to progressively destroying the Kondo resonance; this is sufficient to maintain the π phase shift until large values of V_{sd} of the order of the charging energy. Note that the light signal is very sensitive to the Kondo effect, as ω_0^* and T_K are of the same order of magnitude. Note that the low bias features are not present in Fig. 3(c) due to the small number of points. Fig. 3(c) only presents the general evolution of κ_e and κ_i at a large energy scale (E_c).

We stress that the datas cannot be explained by a resonant-level model, for which Γ does not depend on V_{sd} . From our impurity model, we indeed know that the phase shift from π to 0 occurs for a bias voltage such

that $eV_{sd} \simeq \Gamma$. Then the results of Fig. 5(a) would suggest a constant $\Gamma \simeq E_c$ in the case of a resonant-level model. But such a value of Γ is in contradiction with the Coulomb diamond: we would not have such a resolution if it were the case. This is also in contradiction with the presence of two distinct energy scales in the amplitude of the reflected microwave signal. We remark that there exists a low bias anomaly concerning the phase response in Fig. 5a, which is not present theoretically. From the input-output approach we expect that the phase remains fixed and equal to π at low bias. Near this point, the reflection coefficient is indeed expected to be real and negative. The Fermi liquid corrections [46], which are not taken into account in the input-output approach, may affect the behavior in this region.

It is also interesting to investigate the behavior of the phase as a function of temperature as shown in Fig. 8. One concludes that the phase also allows to probe the Kondo temperature and approaches π for $V_{sd} \rightarrow 0$ when $T < T_K$. A more precise modelling with both the bias voltage and the temperature remains an open question. The phase behavior in the regime $V \sim T_K$ is very sensitive to the precise modelisation of the bias and temperature dependence of Γ , as also observed in the experiment of Ref. [3].

III. COULOMB BLOCKADE REGIME AND INPUT POWER DEPENDENCE

We now discuss amplitude and phase response away from charge degeneracy, at point D well inside the Coulomb diamond (see Figure 2(a)). Here we have $\kappa_i = 1.432 \text{ MHz}$, $\kappa_e = 0.721 \text{ MHz}$ and $\omega_0^* = 7.35076 \text{ GHz}$ at $V_{sd} = 0$ and small input power. By increasing V_{sd} to 0.8 mV , we obtain $\kappa_i = 0.564 \text{ MHz}$, $\kappa_e = 1.358 \text{ MHz}$ and $\omega_0^* = 7.3508 \text{ GHz}$, from a fit result. Figures 9(a) and (b) show the phase and amplitude response at a fixed driving frequency $\omega = \omega_0^*$ at point D. A phase shift is confirmed from bias voltage $V_{sd} = 0$ to $V_{sd} \simeq 0.8 \text{ mV}$. The amplitude sharply goes down for about -15 dB from $V_{sd} = 0$ to $V_{sd} \simeq \pm 0.1 \text{ mV}$, and two side peaks appear around $V_{sd} \simeq \pm 0.15 \text{ mV}$. Then, it continues to go down and two dips appear around $V_{sd} \simeq \pm 0.4 \text{ mV}$, which are again consistent with the charging energy E_c of the quantum dots measured by the Coulomb diamond. At small V_{sd} , this confirms that the Coulomb blockade phenomenon pins the charge fluctuations on the DQD and as a result the photon field is weakly affected by the matter, meaning $\kappa_e \ll \kappa_i$. When the bias voltage increases and compensates the charging energy, there is a revival of charge fluctuations on the DQD then resulting in $\kappa_e \gg \kappa_i$. This explains the jump of the phase from (almost) zero to π at small bias voltages when increasing the microwave power. It is important to note that the cavity is only coupled to the orbital degree of freedom, leading to a phase of zero when $V_{sd} \rightarrow 0$. As a result, it is not sensitive to an eventual spin Kondo effect where the spin and orbital

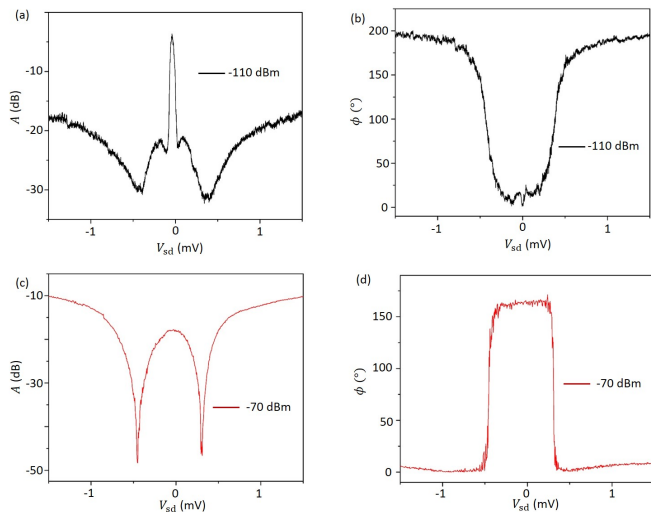


FIG. 9. (color online). Amplitude (a) and phase (b) response as functions of the bias voltage for the point D. Same results when increasing the microwave power.

degrees of freedom are decoupled (resulting from the system composed of the left dot and the left lead alone). A more refined theoretical analysis would be necessary to describe quantitatively the crossover with voltage and to include the charging energy effects.

We then study the power (P) dependence of the resonator response as a function of the bias voltage in the Coulomb blockade regime at the point D. Fixing the driving frequency at resonance $\omega = \omega_0^*$, we show the amplitude response (figures 9(a) and (c)) and the phase response (figures 9(b) and (d)) for two different values of the power. We see that the phase response is in particular drastically modified as the power changes. At high power the amplitude and phase response are close to the ones obtained at point A. This observation can be explained by the fact that the photonic interaction acts as an artificial chemical potential and may compensate the charging at high drive powers. Then the high drive power may bring the system from the Coulomb blockade regime to the resonant regime.

At a mean field level, the equivalent charging energy reads $E_c - \lambda \langle a + a^\dagger \rangle$. In the steady state, the input-output theory allows to relate the drive power to the number of photons in the cavity and ultimately to $\langle a + a^\dagger \rangle$ if we suppose that the steady state of the cavity is a coherent state. Following Ref. [72], we have $P = \hbar \omega \frac{\eta}{4} \langle a^\dagger a \rangle$, where η is the frequency-independent decay rate of the photons in the leads. For a coherent state in the cavity this allows to write $\langle a^\dagger + a \rangle \simeq \sqrt{P/(\hbar \omega \eta)}$. We can then estimate the critical power P_c needed to compensate E_c . We have $E_c = 0.4 meV$, $\omega = 7 GHz$, and we take $\lambda \simeq 0.15 GHz$ and $\eta \simeq 0.1 GHz$. This finally gives $P_c \simeq 10^{-10} W = -70 dBm$, which is consistent with the experimental observations. We note that the

high-power responses at small biases differ slightly from those at point A. This may be linked to additional non-equilibrium effects arising at high power.

We provide additional theoretical derivations in Appendix B, where we also check that bringing the system from a Coulomb blockade regime to a resonant regime is not possible for the points B and C. In this case, the system always remains in a blockade regime as a result of the strong applied orbital magnetic field.

IV. CONCLUSION

In conclusion, we have measured the response of a superconducting resonator capacitively coupled to a biased graphene double quantum dot (DQD). This setup allows to probe dynamically the electronic degrees of freedom with light. We report a full spectroscopic analysis of the resonator's response as a function of the DQD bias and gate voltages. We have furthermore studied the power dependence in the phase and amplitude responses at various points. We explain the experimental findings with a Kondo impurity model entangling the electronic spin and orbital degrees of freedom [27] taking the graphene band structure into account. We assumed that the chemical potential does not lie at the charge neutrality point in order to have a finite density of states in the reservoir leads, making the Kondo energy scale T_K finite. We emphasize that the signatures of such a Kondo effect is visible, both in the phase π at low temperatures and in the dips in the amplitude of the reflected signal occurring roughly at $V_{sd} \sim \pm T_K$. This is also consistent with DC transport data across the DQD, exhibiting a small zero-bias anomaly at $V_{sd} \sim \pm T_K$ which reflects the fact that the Kondo resonance is peaked above the Fermi energy in this system. Note also that the phase of π in the reflected signal is distinct from the phase of $\pi/2$ predicted by the theory in the transmission of light [26]. Light spectroscopy can then probe the dynamical properties of correlated electron phenomena when the light frequency is (almost) synchronized with the typical frequency scale associated with the correlated phenomenon. Our results offer a platform for tunable hybrid quantum electrodynamics and non-equilibrium impurity physics.

We acknowledge discussions with Serge Florens, Takis Kontos, Vladimir Manucharyan and Nicolas Roch on related hybrid systems. We thank Olesia Dmytruk, Pascal Simon and Mircea Trif for discussions. This work was supported by the National Fundamental Research Program (Grant No. 2011CBA00200), National Natural Science Foundation (Grant Nos. 11222438, 10934006, 11274294, 11074243, 11174267 and 91121014). This research has also benefitted from support from the DOE, under the grant DE-FG02-08ER46541. We acknowledge support from the PALM Labex, Paris-Saclay, Grant No. ANR-10-LABX-0039.

Appendix A: General Arguments on the Light-Matter Coupling

The general Hamiltonian of the double dot setup (at any point of the charge stability diagram) takes the form [90] $H_1 = H_L + H_R + H_D + H_T$, where

$$\begin{aligned} H_{l=L,R} &= \sum_{k\sigma} (\epsilon_k + V_l) c_{k\sigma l}^\dagger c_{k\sigma l} \\ H_D &= \sum_{l=L,R} \sum_{p_l\sigma} (\epsilon_{p_l} d_{p_l\sigma}^\dagger d_{p_l\sigma}) + \gamma_L n_L (n_L - 1) + \gamma_R n_R (n_R - 1) + \gamma_M n_L n_R \\ H_T &= \sum_{l=L,R} \sum_{k\sigma} \sum_{p_l} (t_{kn_l} c_{k\sigma l}^\dagger d_{p_l\sigma} + h.c.) + \sum_{p_L p_R \sigma} (t_{p_L p_R} d_{p_L\sigma}^\dagger d_{p_R\sigma} + h.c.). \end{aligned} \quad (A1)$$

The first line describes the electrons in the Left (L) and Right (R) leads, and $c_{k\sigma l}$ ($c_{k\sigma l}^\dagger$) is the annihilation (creation) operator of an electron of spin σ in the mode k and in the lead l . The second line is the Hamiltonian of the two dots: $d_{p_l\sigma}$ ($d_{p_l\sigma}^\dagger$) is the annihilation (creation) operator of an electron of spin σ on the dot $l = L, R$ and at the energy level p_l . Here the γ 's are functions of the capacitances of the tunnel junctions and n_l denotes the number of electrons in the dot l . The last line accounts for lead-dot and inter-dots tunneling events. We now take into account the coupling of the left lead to the superconducting resonator, so that the total Hamiltonian becomes $H = H_1 + H_2$ with

$$H_2 = \omega_0 a^\dagger a + \lambda(a + a^\dagger) \left(\sum_{k\sigma} c_{k\sigma L}^\dagger c_{k\sigma L} \right). \quad (A2)$$

We apply one first unitary transformation $H' = U^\dagger H U$, with

$$U = \exp \left[i\phi \left(\sum_{k\sigma} c_{k\sigma L}^\dagger c_{k\sigma L} \right) \right], \quad (A3)$$

where $\phi = \frac{\lambda(a - a^\dagger)}{i\omega_0}$. We can compute the transformed Hamiltonian H' thanks to the Baker-Campbell-Haussedorff formula $e^X Y e^{-X} = Y + [X, Y] + \frac{1}{2!} [X, [X, Y]] + \frac{1}{3!} [X, [X, [X, Y]]] + \dots$. We then get

$$U^\dagger c_{k\sigma l} U = c_{k\sigma l} e^{i\phi} \quad (A4)$$

$$U^\dagger (\omega_0 a^\dagger a) U = -\lambda(a + a^\dagger) \left(\sum_{k\sigma} c_{k\sigma L}^\dagger c_{k\sigma L} \right) \quad (A5)$$

$$U^\dagger \left[\lambda(a + a^\dagger) \left(\sum_{k\sigma} c_{k\sigma L}^\dagger c_{k\sigma L} \right) \right] U = \frac{2\lambda^2}{\omega_0} \left(\sum_{k\sigma} c_{k\sigma L}^\dagger c_{k\sigma L} \right)^2. \quad (A6)$$

Assuming small fluctuations concerning the total number of conduction electrons, the right hand side of Eq. (6) is almost a constant, so that the resulting Hamiltonian reads $H' = H_L + H_R + H_D + H'_T + \omega_0 a^\dagger a$, where we have

$$H'_T = \sum_{k\sigma} \sum_{p_L} (t_{kp_L} c_{k\sigma L}^\dagger d_{p_L\sigma} e^{-i\phi} + h.c.) + \sum_{k\sigma} \sum_{p_R} (t_{kp_R} c_{k\sigma R}^\dagger d_{p_R\sigma} + h.c.) + \sum_{p_L p_R \sigma} (t_{p_L p_R} d_{p_L\sigma}^\dagger d_{p_R\sigma} + h.c.). \quad (A7)$$

This unitary transformation has suppressed the explicit coupling between the left lead and the resonator. The tunneling terms from the Left lead to the Left dot have moreover acquired a phase which depends on the state of the resonator.

We apply then a second unitary transformation $\tilde{H} = V^\dagger H' V$, with

$$V = \exp \left[i\phi \left(\sum_{p_L\sigma} d_{p_L\sigma}^\dagger d_{p_L\sigma} \right) \right]. \quad (A8)$$

After similar calculations, the resulting Hamiltonian reads $\tilde{H} = H_L + H_R + \tilde{H}_D + \tilde{H}_T + \omega_0 a^\dagger a$, where we have

$$\begin{aligned}\tilde{H}_D &= H_D - \lambda(a + a^\dagger) \left(\sum_{p_L \sigma} d_{p_L \sigma}^\dagger d_{p_L \sigma} \right) \\ \tilde{H}_T &= \sum_{l=L,R} \sum_{k\sigma} \sum_{p_l} (t_{kp_l} c_{k\sigma l}^\dagger d_{p_l \sigma} + h.c.) + \sum_{p_L p_R \sigma} (t_{p_L p_R} d_{p_L \sigma}^\dagger d_{p_R \sigma} e^{-i\phi} + h.c.).\end{aligned}\quad (\text{A9})$$

In this final form, the mode of the resonator is coupled to the energy levels of the Left dot. Additionally, the tunneling term between the dots has acquired a phase which depends on the \hat{p} operator of the mode.

This analysis implies that the form of the reflection coefficient S_{11} in Eq. (5) of the main text is valid for all the points in the charge stability diagram.

Appendix B: High power regime

1. General arguments

For large drive, we decompose the photon annihilation operator as $a = \langle a \rangle + d$. The first part $\langle a \rangle$ is determined by the strength of the drive field and the damping rate, and we suppose that steady state of the cavity is a coherent state. We see that the constant semi-classical part of the drive $\langle a + a^\dagger \rangle$ acts as a chemical potential on the Left dot. Increasing the drive power will then move the system on the honeycomb phase diagram of the double dot. Following Ref. [74] the chemical potentials of the two dots μ_L and μ_R read as a function of the number of electrons on the dots (N_L and N_R),

$$\mu_L(N_L, N_R) = \left(N_L - \frac{1}{2} - \lambda \langle a + a^\dagger \rangle \right) E_{C_L} + N_R E_{C_m} - \frac{1}{|e|} (C_{gL} V_{LP} E_{C_L} + C_{gR} V_{RP} E_{C_m}) \quad (\text{B1})$$

$$\mu_R(N_L, N_R) = \left(N_R - \frac{1}{2} \right) E_{C_R} + N_L E_{C_m} - \frac{1}{|e|} (C_{gL} V_{LP} E_{C_m} + C_{gR} V_{RP} E_{C_R}), \quad (\text{B2})$$

where E_{C_j} is the charging energy of the individual dot j , E_{C_m} is the electrostatic coupling energy, C_j (C_{gj}) is the capacitance coupling the dot j to the neighboring lead (gate), and C_m is the capacitance which couples the dots together. The Left and Right gate voltages are denoted by V_{LP} and V_{RP} . The effect of the driving can be absorbed into the definition of new gates voltages V'_{LP} and V'_{RP} ,

$$V'_{LP} = V_{LP} - \frac{\lambda \langle a + a^\dagger \rangle |e|}{C_{gL} \left(E_{C_L} - \frac{E_{C_m}^2}{E_{C_R}} \right)} \quad (\text{B3})$$

$$V'_{RP} = V_{RP} - \frac{\lambda \langle a + a^\dagger \rangle |e|}{C_{gR} \left(E_{C_m} - \frac{E_{C_L} E_{C_R}}{E_{C_m}} \right)}. \quad (\text{B4})$$

Driving the system at high power allows to move the state of the system on the honeycomb phase diagram along a line characterized by the equations (B3) and (B4). This corresponds to

$$\frac{\delta V_{RP}}{\delta V_{LP}} = \frac{C_{gL}}{C_{gR}} \frac{E_{C_m}}{E_{C_R}}. \quad (\text{B5})$$

Such a line has a slope which is the opposite of the line of degeneracy between the states (N, M) and $(N, M + 1)$ (the lines where lies the point B).

2. Theory at Point A

We can see from Fig. 10 that driving the cavity may bring the system at resonance (close to the point A).

Now we give an estimate for the input power that allows to make this transition from the Coulomb Blockade regime to the resonant regime. In the steady state, the input-output theory allows to relate the drive power to the number of

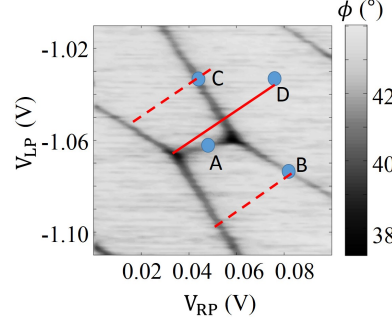


FIG. 10. (color online). Effect of the driving on the state of the system. The full red line shows the shift in the phase diagram induced by the drive at point D. The dotted red lines accounts for the shifts caused by the drive from the points B and C.

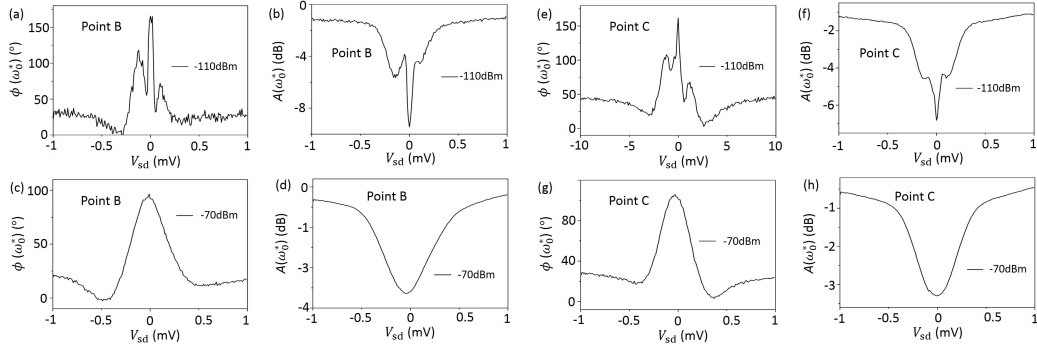


FIG. 11. (color online). Amplitude (a) and (e) and phase (b) and (f) responses as functions of the bias voltage for the point B and C. Amplitude (c) and (g) and phase (d) and (h) responses when increasing the microwave power for the point B and C.

photons in the cavity and ultimately to $\langle a + a^\dagger \rangle$. Following Eq. (E45) of Ref. [72], we have $P = (\hbar\omega\eta/4)\langle a^\dagger a \rangle$, where η is the decay rate of the photons in the leads (assumed to be independent over the range of frequencies relevant to the cavity - Markov approximation). If we suppose that the steady state of the cavity is a coherent state, we have

$$\langle a^\dagger + a \rangle \simeq \sqrt{\frac{P}{\hbar\omega\eta}}. \quad (\text{B6})$$

We can then estimate the critical power P_c needed to compensate E_c . We have $E_c = 0.4\text{meV}$, $\omega = 7\text{GHz}$, and we take $\lambda \simeq 0.15\text{GHz}$ and $\eta \simeq 0.1\text{GHz}$. This finally gives

$$P_c \simeq -70\text{dBm}. \quad (\text{B7})$$

This result is consistent with the experimental observations.

3. Experimental Checks at points B and C

Bringing the system from a Coulomb blockade regime to a resonant regime is not possible for the points B and C, as illustrated by the dotted red lines in Fig. 10. The system always stays in a blockade regime. This behavior is verified experimentally, as shown in Fig. 11. Driving the system at high power does not affect (much) the response of the reflection coefficient.

-
- [1] A. Dousse, L. Lanco, J. Suffczynski, E. Semenova, A. Miard, A. Lemaître, I. Sagnes, C. Roblin, J. Bloch, and P. Senellart, *Phys. Rev. Lett.* **101**, 267404 (2008).
 - [2] Z.-L. Xiang, S. Ashhab, J. Q. You, and F. Nori, *Rev. Mod. Phys.* **85**, 623 (2013).
 - [3] M. R. Delbecq, V. Schmitt, F. D. Parmentier, N. Roch, J. J. Viennot, G. Fève, B. Huard, C. Mora, A. Cottet, and T. Kontos, *Phys. Rev. Lett.* **107**, 256804 (2011).
 - [4] K. D. Petersson, L. W. McFaul, M. D. Schroer, M. Jung, J. M. Taylor, A. H. Houck, and J. R. Petta, *Nature* **490**, 380 (2012).
 - [5] T. Frey, P. J. Leek, M. Beck, A. Blais, T. Ihn, K. Ensslin, and A. Wallraff, *Phys. Rev. Lett.* **108**, 046807 (2012).
 - [6] T. Frey, P. J. Leek, M. Beck, J. Faist, A. Wallraff, K. Ensslin, T. Ihn, and M. Büttiker, *Phys. Rev. B* **86**, 115303 (2012).
 - [7] H. Toida, T. Nakajima, and S. Komiyama, *Phys. Rev. Lett.* **110**, 066802 (2013).
 - [8] M. Delbecq, L. Bruhat, J. Viennot, S. Datta, A. Cottet, and T. Kontos, *Nat. Commun.* **4**, 1400 (2013).
 - [9] G.-W. Deng, D. Wei, J. Johansson, M.-L. Zhang, S.-X. Li, H.-O. Li, G. Cao, M. Xiao, T. Tu, G.-C. Guo, H.-W. Jiang, F. Nori, and G.-P. Guo, *Phys. Rev. Lett.* **115**, 126804 (2015).
 - [10] Y.-Y. Liu, K. D. Petersson, J. Stehlik, J. M. Taylor, and J. R. Petta, *Phys. Rev. Lett.* **113**, 036801 (2014).
 - [11] G.-W. Deng, D. Wei, S.-X. Li, J. R. Johansson, W.-C. Kong, H.-O. Li, G. Cao, M. Xiao, G.-C. Guo, F. Nori, H.-W. Jiang, and G.-P. Guo, *Nano Lett.* **15**, 6620 (2015).
 - [12] L. Childress, A. Sorensen, and M. Lukin, *Phys. Rev. A* **69**, 042302 (2004).
 - [13] Z.-R. Lin, G.-P. Guo, T. Tu, F.-Y. Zhu, and G.-C. Guo, *Phys. Rev. Lett.* **101**, 230501 (2008).
 - [14] C. Bergenfeldt, P. Samuelsson, B. Sothmann, C. Flindt, and M. Büttiker, *Phys. Rev. Lett.* **112**, 076803 (2014).
 - [15] J. J. Viennot, M. R. Delbecq, M. C. Dartiailh, A. Cottet, and T. Kontos, *Phys. Rev. B* **89**, 165404 (2014).
 - [16] J. Basset, D.-D. Jarausch, A. Stockklauser, T. Frey, C. Reichl, W. Wegscheider, T. M. Ihn, K. Ensslin, and A. Wallraff, *Phys. Rev. B* **88**, 125312 (2013).
 - [17] X. Hu, Y.-X. Liu, and F. Nori, *Phys. Rev. B* **86**, 035314 (2012).
 - [18] C. Bergenfeldt and P. Samuelsson, *Phys. Rev. B* **87**, 195427 (2013).
 - [19] N. Lambert, C. Flindt, and F. Nori, *EPL* **103**, 17005 (2013).
 - [20] L. D. Contreras-Pulido, C. Emary, T. Brandes, and R. Aguado, *New J. Phys.* **15**, 095008 (2013).
 - [21] J. Basset, A. Stockklauser, D.-D. Jarausch, T. Frey, C. Reichl, W. Wegscheider, A. Wallraff, K. Ensslin, and T. Ihn, *Appl. Phys. Lett.* **105**, 063105 (2014).
 - [22] Y.-Y. Liu, K. D. Petersson, J. Stehlik, J. M. Taylor, and J. R. Petta, *Science* **347**, 285 (2015).
 - [23] A. Stockklauser, V. F. Maisi, J. Basset, K. Cujia, C. Reichl, W. Wegscheider, T. Ihn, A. Wallraff, and K. Ensslin, *arXiv:1504.0549* (2015).
 - [24] L. Henriët, A. N. Jordan, and K. Le Hur, *Phys. Rev. B* **92**, 125306 (2015).
 - [25] J. M. Raimond, M. Brune, and S. Haroche, *Rev. Mod. Phys.* **73**, 565 (2001).
 - [26] M. Schirò and K. Le Hur, *Phys. Rev. B* **89**, 195127 (2014).
 - [27] L. Borda, G. Zarand, W. Hofstetter, B. Halperin, and J. von Delft, *Phys. Rev. Lett.* **90**, 026602 (2003).
 - [28] K. Le Hur, P. Simon, and L. Borda, *Phys. Rev. B* **69**, 045326 (2004).
 - [29] K. Le Hur, P. Simon, and D. Loss, *Phys. Rev. B* **75**, 035332 (2007).
 - [30] R. Lopez, D. Sanchez, M. Lee, M.-S. Choi, P. Simon, and K. Le Hur, *Phys. Rev. B* **71**, 115312 (2005).
 - [31] A. J. Keller, S. Amasha, I. Weymann, C. P. Moca, I. G. Rau, J. A. Katine, H. Shtrikman, G. Zarand, and D. Goldhaber-Gordon, *Nature Phys.* **10**, 145 (2014).
 - [32] A. Makarovski, J. Liu, and G. Finkelstein, *Phys. Rev. Lett.* **99**, 066801 (2007).
 - [33] S. Sasaki, S. Amaha, N. Asakawa, M. Eto, and S. Tarucha, *Phys. Rev. Lett.* **93**, 017205 (2004).
 - [34] T. Delattre, C. Feuillet-Palma, L. Herrmann, P. Morfin, J.-M. Berroir, G. Fève, B. Plaçaïs, D. Glatthli, M.-S. Choi, C. Mora, and T. Kontos, *Nature Physics* **5**, 208 (2009).
 - [35] P. Jarillo-Herrero, J. Kong, H. S. van der Zant, C. Dekker, L. P. Kouwenhoven, and S. D. Franceschi, *Nature* **434**, 484 (2005).
 - [36] J. Basset, A. Y. Kasumov, C. P. Moca, G. Zaránd, P. Simon, H. Bouchiat, and R. Deblock, *Phys. Rev. Lett.* **108**, 046802 (2012).
 - [37] R. Delagrange, D. J. Luitz, R. Weil, A. Kasumov, V. Meden, H. Bouchiat, and R. Deblock, *Phys. Rev. B* **91**, 241401 (R) (2015).
 - [38] R. Shang, H.-O. Li, G. Cao, G. Yu, M. Xiao, T. Tu, G.-C. Guo, H. Jiang, A.M.Chang, and G.-P. Guo, *Phys. Rev. B* **91**, 245102 (2015).
 - [39] A. K. Mitchell, M. R. Galpin, and D. E. Logan, *EPL (Europhysics Letters)* **76**, 95 (2006).
 - [40] J. J. Viennot, M. C. Dartiailh, A. Cottet, and T. Kontos, *Science* **349**, 408 (2015).
 - [41] C. Arnold, J. Demory, V. Loo, A. Lemaître, I. Sagnes, M. Glazov, O. Krebs, P. Voisin, P. Senellart, and L. Lanco, *Nat Commun* **6** (2015).
 - [42] M. Kulkarni, O. Cotlet, and H. E. Türeci, *Phys. Rev. B* **90**, 125402 (2014).
 - [43] K. Le Hur, L. Henriët, A. Petrescu, K. Plekhanov, G. Roux, and M. Schirò, *arXiv:1505.00167* (2015).

- [44] A. J. Keller, S. Amasha, I. Weymann, C. P. Moca, I. G. Rau, J. A. Katine, H. Shtrikman, G. Zarand, and D. Goldhaber-Gordon, *Nat Phys* **10**, 145 (2014).
- [45] J. Kondo, *Prog. Theor. Phys.* **32** (1), 37 (1964).
- [46] P. Nozières, *Journal of Low Temperature Physics* **17**, 31 (1974).
- [47] K. G. Wilson, *Rev. Mod. Phys.* **47**, 773 (1975).
- [48] N. Andrei, *Phys. Rev. Lett.* **45**, 379 (1980).
- [49] A. M. Tsvelick and P. B. Wiegmann, *Advances in Physics* **32**, 453 (1983).
- [50] I. Affleck, *Acta Phys. Polon. B26*, 1869 (1995).
- [51] A. C. Hewson, *The Kondo Problem to Heavy Fermions* (Cambridge University Press, 1997).
- [52] D. Goldhaber-Gordon, D. H. Shtrikman, D. Mahalu, D. Abusch-Magder, U. Meirav, and M. A. Kastneret, *Nature* **391**, 156 (1998).
- [53] W. G. van der Wiel, S. D. Franceschi, T. Fujisawa, J. M. Elzerman, S. Tarucha, and L. P. Kouwenhoven, *Science*.
- [54] L. Kouwenhoven and L. Glazman, *Physics World* **14**, No 1, 33 (2001).
- [55] I. G. Rau, S. Amasha, Y. Oreg, and D. Goldhaber-Gordon, arXiv:1309.7737 and "Understanding Quantum Phase Transitions" (series: Condensed Matter Physics, Nov. 2 2010) by CRC Press.
- [56] R.-N. Shang, H.-O. Li, G. Cao, G.-D. Yu, M. Xiao, T. Tu, G.-C. Guo, H.-W. Jiang, A. Chang, and G.-P. Guo, *Phys. Rev. B* **91**, 245102 (2015).
- [57] L.-J. Wang, G.-P. Guo, D. Wei, G. Cao, T. Tu, M. Xiao, G.-C. Guo, and A. M. Chang, *Appl. Phys. Lett.* **99**, 112117 (2011).
- [58] L.-J. Wang, H.-O. Li, T. Tu, G. Cao, C. Zhou, X.-J. Hao, Z. Su, M. Xiao, G.-C. Guo, A. M. Chang, and G.-P. Guo, *Appl. Phys. Lett.* **100**, 022106 (2012).
- [59] J.-H. Chen, L. Li, W. G. Cullen, E. D. Williams, and M. S. Fuhrer, *Nature Physics* **7**, 535 (2011).
- [60] R. Leturcq, L. Schmid, K. Ensslin, Y. Meir, D. C. Driscoll, and A. C. Gossard, *Phys. Rev. Lett.* **95**, 126603 (2005).
- [61] K. Le Hur, *Phys. Rev. B* **85**, 140506 (R) (2012).
- [62] M. Goldstein, M. H. Devoret, M. Houzet, and L. I. Glazman, *Phys. Rev. Lett.* **110**, 017002 (2013).
- [63] I. Snyman and S. Florens, arXiv:1503.05708.
- [64] M. Haeblerlein, F. Deppe, A. Kurcz, J. Goetz, A. Baust, P. Eder, K. Fedorov, M. Fischer, E. P. Menzel, M. J. Schwarz, F. Wulschner, E. Xie, L. Zhong, E. Solano, A. Marx, J.-J. Garca-Ripoll, and R. Gross, arXiv:1506.09114 (2015).
- [65] C. Altimiras, O. Parlavecchio, P. Joyez, D. Vion, P. Roche, D. Esteve, and F. Portier, *Appl. Phys. Lett.* **103**, 212601 (2013).
- [66] B. Peropadre, J. Lindkvist, I.-C. Hoi, C. Wilson, J. Garcia-Ripoll, P. Delsing, and G. Johansson, *New J. Phys.* **15**, 035009 (2013).
- [67] C. Latta, F. Haupt, M. Hanl, A. Weichselbaum, M. Claassen, W. Wuester, P. Fallahi, S. Faelt, L. Glazman, J. von Delft, H. E. Türeci, and A. Imamoglu, *Nature* **474**, 627 (2011).
- [68] A. Rosch, J. Kroha, and P. Wölfle, *Phys. Rev. Lett.* **87**, 156802 (2001).
- [69] A. Kaminski, Y. Nazarov, and L. Glazman, *Phys. Rev. B* **62**, 8154 (2000).
- [70] C.-H. Chung, K. Le Hur, M. Vojta, and P. Woelfle, *Phys. Rev. Lett.* **102**, 216803 (2009).
- [71] C. W. Gardiner and M. J. Collett, *Phys. Rev. A* **31**, 3761 (1985).
- [72] A. Clerk, M. Devoret, S. Girvin, F. Marquardt, and R. Schoelkopf, *Rev. Mod. Phys.* **82**, 1155 (2010).
- [73] M.-L. Zhang, G.-W. Deng, S.-X. Li, H.-O. Li, G. Cao, T. Tu, M. Xiao, G.-C. Guo, H.-W. Jiang, I. Siddiqi, and G.-P. Guo, *Appl. Phys. Lett.* **104**, 083511 (2014).
- [74] W. G. van der Wiel, S. D. Franceschi, J. M. Elzerman, T. Fujisawa, S. Tarucha, and L. P. Kouwenhoven, *Rev. Mod. Phys.* **75**, 1 (2002).
- [75] A. H. Castro Neto, F. Guinea, N. M. R. Peres, K. S. Novoselov, and A. K. Geim, *Rev. Mod. Phys.* **81**, 109 (2009).
- [76] R. Egger and O. Gogolin, *Eur. Phys. J. B* **3** (3), 281 (1998).
- [77] K. Le Hur, S. Vishveshwara, and C. Bena, *Phys. Rev. B* **77**, 041406 (R) (2008).
- [78] P. Nozières, *Journ. of Low Temperature Physics* **17**, 31 (1974).
- [79] I. Affleck and A. Ludwig, *Phys. Rev. B* **48**, 7297 (1993).
- [80] C. Mora, P. Vitushinsky, X. Leyronas, A. A. Clerk, and K. Le Hur, *Phys. Rev. B* **80**, 155322 (2009).
- [81] M. Li and K. Le Hur, *Phys. Rev. Lett.* **93**, 176802 (2004).
- [82] A. J. Leggett, S. Chakravarty, A. T. Dorsey, M. P. A. Fisher, A. Garg, and W. Zwerger, *Rev. Mod. Phys.* **67**, 725 (1995).
- [83] U. Weiss, *Quantum Dissipative Systems*, Fourth Edition, World Scientific, 2012.
- [84] K. Le Hur, *Annals of Physics* **323**, 2208 (2008).
- [85] P. P. Orth, A. Imambekov, and K. Le Hur, *Phys. Rev. B* **87**, 014305 (2013).
- [86] L. Henriët, Z. Ristivojevic, P. P. Orth, and K. Le Hur, *Phys. Rev. A* **90**, 023820 (2014).
- [87] C. R. Xu and M. G. Vavilov, *Phys. Rev. B* **87**, 035429 (2013).
- [88] S. Bera, A. Nazir, A. W. Chin, H. U. Baranger, and S. Florens, *Phys. Rev. B* **90**, 075110 (2014).
- [89] P. Dutt, J. Koch, J. Han, and K. Le Hur, *Annals of Physics* **326**, 2963 (2011).
- [90] R. Ziegler, C. Bruder, and H. Schoeller, *Phys. Rev. B* **62**, 1961 (2000).